AMERICAN SCIENTIFIC PUBLISHERS

Science of Advanced Materials
Vol. 8, pp. 11–16, 2016
www.aspbs.com/sam

Performance Enhancement in Thin Film Solid Oxide Fuel Cells Using Metal-Mixed Ionic Electronic Conductors Bilayer Anode

Seungtak Noh[1], Gu Young Cho[1], Yoon Ho Lee[1], Wonjong Yu[1], Jihwan An[2,*], and Suk Won Cha[1,*]

[1] *School of Mechanical and Aerospace Engineering, Seoul National University, San 56-1, Daehak-Dong, Gwanak-Gu, Seoul 151-742, Republic of Korea*
[2] *Manufacturing Systems and Design Engineering Programme, Seoul National University of Science and Technology, 232 Gongneung-Ro, Nowon-Gu, Seoul 139-743, Republic of Korea*

ABSTRACT

A 70 nm-thick Ni layer deposited between the NiO-gadolinia doped ceria (NiO-GDC) anode and the anodic aluminum oxide (AAO) substrate successfully enhanced the electrochemical performance of thin film solid oxide fuel cells (TF-SOFCs) using the sputtering technique. The thickness ratio between the NiO-GDC and Ni layer on the cell performance was investigated. The TF-SOFCs with sputtered 210 nm-thick NiO-GDC and 70 nm-thick Ni layers exhibited maximum power density of 170 mW/cm^2 at 500 °C, which was about two times higher than those without Ni layers (80 mW/cm^2). The electrochemical impedance spectroscopy showed that the performance improvement mostly stems from two factors: the reduced ohmic and anodic activation resistances and the improved anodic kinetics. When the NiO-GDC layer is too thin (70 nm), the ionic conduction in the NiO-GDC layer became sluggish. Therefore, the maximum power density decreased to 132 mW/cm^2. Thus, we can conclude a proper thickness ratio between the NiO-GDC and Ni layers is required to maximize cell performance.

KEYWORDS: Nickel, Nickel Oxide-Gadolinia-Doped Ceria, Thin Film-Solid Oxide Fuel Cells, Anode, Sputter.

ARTICLE

1. INTRODUCTION

Solid oxide fuel cells (SOFCs), which employ solid ceramic materials as electrolytes, have received considerable attention due to fuel flexibility and wide catalyst selection.[1] The high operating temperature of SOFCs (i.e., 800–1000 °C), however, has many drawbacks like fast thermal degradation, expensive thermal resistance materials, sealing issues, and long start-up times.[1]

Various research has been conducted to reduce the operating temperature of the thin film SOFC (TF-SOFC).[2–7] In TF-SOFCs, the ohmic resistance decreases due to the reduction in electrolyte thickness. Additionally, nano-scale particles fabricated by the vacuum deposition technique (e.g., physical vapor deposition (PVD) and chemical vapor deposition (CVD)) increase the electrochemically active specific area to reduce the activation resistance of the cell. Therefore, the performance drop at low operating temperatures can be compensated.[8, 9]

Another way to reduce the operating temperature is to choose electrochemically active materials even at low electrode temperatures. For fuel cells, an electrochemical reaction can only take place at triple phase boundaries (TPBs) where electrolyte, electrode, and gas are in contact. An increase in reaction rate can be achieved by maximizing the triple phase boundary (TPB) density.[1] The employment of mixed ionic electronic conductor (MIECs) electrodes such as nickel oxide/yttria-stabilized zirconia (NiO-YSZ), nickel oxide/gadolinia-doped ceria (NiO-GDC), and nickel oxide/samaria-doped ceria (NiO-SDC) for the anode in addition to lanthanum strontium cobalt ferrite (LSCF) and lanthanum strontium manganite (LSM) for the cathode may be a solution, because TPB density can be increased from the electrolyte/electrode interface (2D) to the entire electrode region (3D). As a result, activation loss can be significantly reduced by using MIECs.[10–13]

Among the MIEC anode materials mentioned previously, NiO-YSZ matches well with YSZ electrolyte's thermal expansion and has chemical stability over a wide temperature range.[14] Nevertheless, the ionic conduction in YSZ composite is sluggish at low temperatures (400–600 °C) and the ohmic resistance significantly increases. On the other hand, GDC has higher ionic

*Authors to whom correspondence should be addressed.
Emails: jihwanan@seoultech.ac.kr, swcha@snu.ac.kr
Received: 15 March 2015
Accepted: 15 July 2015

conductivity than YSZ,[1, 10] which may make GDC more suitable for the application of low temperature SOFCs.

Compared to pure nickel, NiO-GDC has been believed to enlarge TPB density and lower faradaic resistance.[15] The electrical conductivity of NiO-GDC, however, is significantly smaller than that of pure nickel at low temperatures. Thus, the resultant high ohmic resistance of the NiO-GDC electrode could be problematic.[12, 15, 16]

In the present study, the TF-SOFCs comprised of (cathode)Pt | YSZ | NiO-GDC | Ni(anode) were fabricated. In order to improve the electrical conductivity of the NiO-GDC anode, we deposited Ni current collection layer between the NiO-GDC film and nanoporous AAO substrate.[17] Several TF-SOFCs with different Ni to NiO-GDC bilayer anode thickness ratio were fabricated and analyzed for the cell performance of both Ni and NiO-GDC layers thickness. As mentioned above, ohmic loss in the bilayer anode was influenced by the additional Ni layer thickness. The NiO-GDC layer thickness also affected the ohmic resistance size. Electrochemical characterizations such as open circuit voltage measurement, current–voltage characterization, and electrochemical impedance spectroscopy (EIS) were evaluated at 500 °C.

2. EXPERIMENTAL DETAILS

We utilized commercial AAO membranes (Synkera Technology Inc., U.S.A.) with 80 nm pore diameter and 100 μm thick substrates of the TF-SOFCs. As shown in Figure 1, Ni, NiO-GDC, YSZ, and Pt layers were sequentially deposited on a 1×1 cm^2 AAO membrane substrate. The TF-SOFCs with anodes of different Ni/NiO-GDC thickness ratios and same total thickness were prepared to investigate the effect of the Ni layer on the cell performance. Detailed information is provided in Table I. We named the three TF-SOFCs as cell 1, cell 2, and cell 3, respectively.

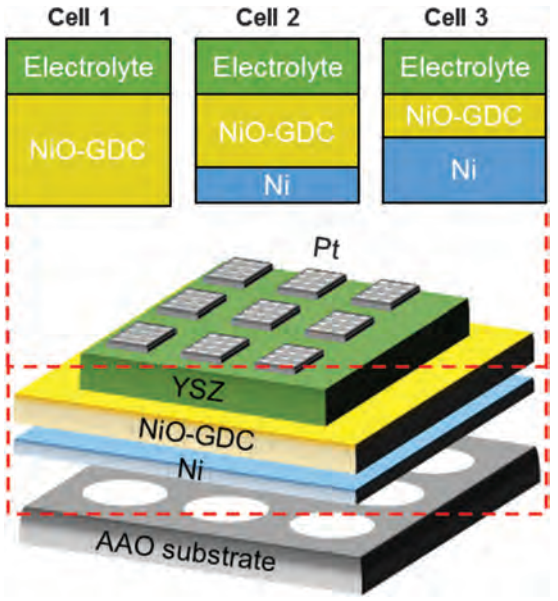

Fig. 1. Schematic of TF-SOFCs.

Table I. Detailed information about fabricated cells.

	Thickness (nm)			
	Anode		Electrolyte	Cathode
	Ni	NiO-GDC	YSZ	Pt
Cell 1	0	280	600	150
Cell 2	70	210	600	150
Cell 3	210	70	600	150

A thin Ni layer was deposited on the AAO substrate using a metal Ni target (99.99%, RnD Korea, Korea) by direct current (DC) magnetron sputtering at an Ar pressure of 4 Pa. (99.999%) with sputtering power set to 100 W. Subsequently, a dense NiO-GDC layer was deposited on the Ni layer using commercial NiO-GDC targets (50:50 weight percent, NiO-$(CeO_2)_{0.9}$ $(GdO_{1.5})_{0.1}$, RnD Korea, Korea) by radio frequency (RF) magnetron sputtering at a mixed Ar/O_2 gas (O_2/Ar ratio: 20%) at 0.93 Pa and sputtering power set to 50 W. The Ni to NiO-GDC thickness ratios were controlled by the sputtering time.

A RF sputtering power of 200 W was applied to the Zr–Y alloy target (16 atomic percent Y, 84 atomic percent Zr, Advantec Korea, Korea) with a mixed Ar/O_2 gas at 0.67 Pa. A fully dense YSZ electrolyte was successfully deposited on the top of the bilayer anode. Finally, a porous Pt cathode was sputtered by using DC plasma at 100 W under Ar pressure of 12 Pa. The effective area was controlled to 0.1×0.1 cm^2 using a physical shadow mask. For each sputtering process, the distance between the target and the substrate was maintained at 80 mm and the substrate temperature was set at room temperature.

To investigate the chemical composition ratio of the NiO-GDC layer, field emission scanning electron microscopy with energy dispersive X-ray spectroscopy (FESEM-EDS, S-4800, Hitachi, Japan) analysis was conducted. Cross-sectional structural images of TF-SOFCs were acquired to measure the thickness of each layer by using focused ion beam-scanning electron microscopy (FIB-SEM, Quanta 3D FEG, FEI company, U.S.A.) at the operating voltage of 5 kV.

The electrochemical performance of the cells was measured with a custom-made test station in an electric furnace at 500°C.[18–21] Dry hydrogen (99.999%) was supplied to the anode side with a flow rate of 100 sccm, and the cathode side was exposed to the ambient atmosphere. For the current collection, a hardened-steel probe (Leeno Inc., Korea) was directly contacted to the cathode while a 0.5 mm diameter silver wire was connected to the anode using silver paste (597A, Aremco products, U.S.A.).

Polarization curves and impedance spectra were obtained using an impedance analyzer (Solartron analytical

1260/1287, Solatron, U.K.). The polarization curves were acquired by using the potentiodynamic technique with a 30 mV/s scan rate. Electrochemical impedance spectroscopy (EIS) was conducted at OCV with the AC voltage at 30 mV amplitude in the 2 Hz to 1 MHz frequency range.

3. RESULTS AND DISCUSSION

Figure 2 presents the surface morphology and chemical composition of the NiO-GDC film deposited on the AAO template. As shown in Figure 2(a), the NiO-GDC film deposited on the AAO substrate shows fine-grained and nanoporous morphology. Figures 2(b–d) present the EDS composition mapping of Ni, Ce, and Gd elements at the surface shown in Figure 2(a), visualized by different colors. As expected, Ni, Ce, and Gd atoms are uniformly distributed on the surface of NiO-GDC films, which implies TPB sites are also uniformly distributed over the entire NiO-GDC electrode. The chemical composition ratios of the NiO-GDC film are obtained. The measured atomic concentration of Ni on the film surface is 26.5%, which is close to the values presented in previous reports and sufficient enough to facilitate hydrogen oxidation at the TPB.[22, 23] The Ce concentration (22.4%) to Gd content (2.54%) ratio of the film is 8.80, which is similar to that of the target (9:1). This result indicates that the chemical composition ratio of NiO-GDC composites is successfully maintained during the sputtering process.

Cross-sectional images of the cells obtained using FIB-SEM are shown in Figures 3(a–c). In all figures, there are over four layers in the cells. Approximately 150 nm-thick porous Pt cathode is expected to provide an oxygen path for the oxygen reduction reaction (ORR) and maximize TPBs. Additionally, the approximately 600 nm-thick YSZ electrolyte layer has a fully dense structure. A few defects are discernible in Figures 3(b and c), but do not form a percolating path. From OCV values and I–V curves discussed in the following section, we confirmed that the isolated defects do not result in leakage current problem. The bottom-most AAO substrate seems to have several pores with 80-nm diameter, which are regarded as hydrogen gas channels. NiO-GDC or Ni/NiO-GDC bilayer anodes are shown between the AAO template and YSZ electrolyte. In addition, Ni/NiO-GDC interfaces were highlighted. A relatively bright layer above the AAO substrate was the Ni layer and the slightly dark thin layer above the Ni layer was the NiO-GDC MIECs layer. There is no noticeable difference in the surface morphology of the cathode and electrolyte between the TF-SOFCs. Therefore, the differences in electrochemical characteristics of the TF-SOFCs are assumed to originate from different anode structures.

Polarization curves of the TF-SOFCs are presented in Figure 4. First, the OCV values were 1.12, 1.13, and 1.13 V for cell 1, cell 2 and cell 3, respectively, at 500 °C. These were similar to previous values in μ-SOFC studies using nanoporous AAO substrate based YSZ electrolytes.[3, 19, 20, 24–26] These results indicate that the pinhole free and gas-tight YSZ thin film electrolyte was successfully deposited on the nano-porous NiO-GDC or

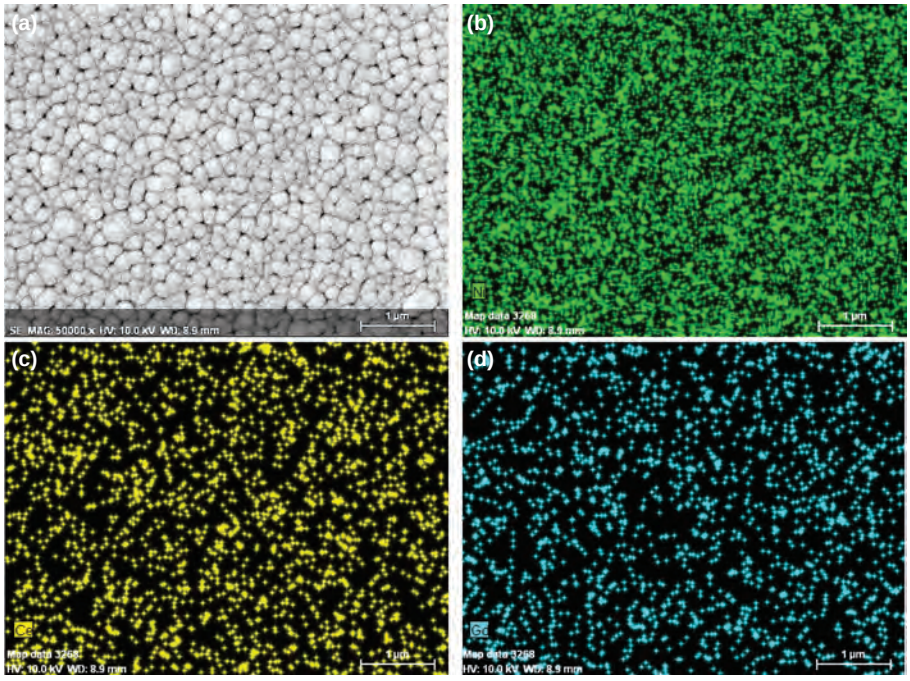

Fig. 2. FESEM-EDS data of the sputtered NiO-GDC film deposited on the AAO substrate (a) magnified FESEM image and (b–d) EDS composition maps of the film.

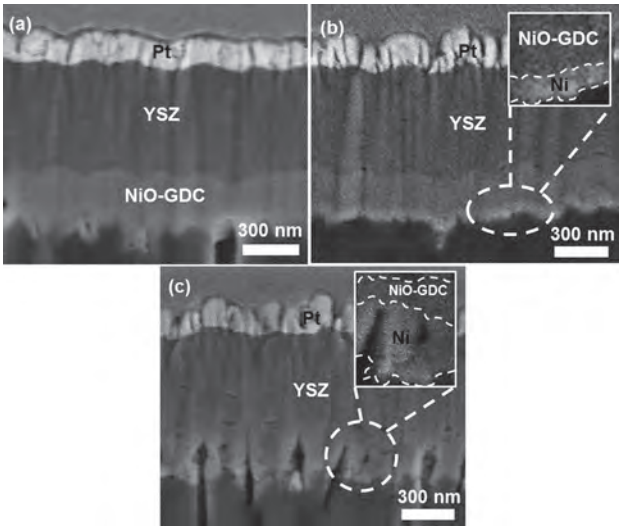

Fig. 3. FIB cross-sectional images of sputtered NiO-GDC anode cells (a) without Ni layer (cell 1) and (b–c) with Ni layer (cell 2–3).

Ni/NiO-GDC anode. Additionally, similar OCVs of the TF-SOFCs mean that variations in Ni/NiO-GDC thickness ratios had negligible effects on OCVs.

The maximum power densities of cell 1, cell 2 and cell 3 were 80, 170, and 132 mW/cm^2, respectively. Compared to cell 1, cell 2 exhibits more than a two-fold increase in maximum power density (80 mW/cm^2 → 170 mW/cm^2) when the 70 nm-thick Ni layer was added and the NiO-GDC layer thickness was decreased from 280 nm to 210 nm. Cell 3, however, exhibited lower performance than cell 2 (170 mW/cm^2 → 132 mW/cm^2), although the Ni layer thickness increased.

To investigate the resistances from the individual fuel cell processes, impedance spectra nyquist plots of the cells with different Ni/NiO-GDC thickness-ratios were obtained under 0.5 V bias at 500 °C (Fig. 5). The impedance spectra resistances were calculated by fitting to the equivalent circuit model and presented in Table II.[3, 20] In the equivalent circuit model, R1, R2, R3, and R4 represent the electronic resistance, ionic resistance, anode polarization resistance,

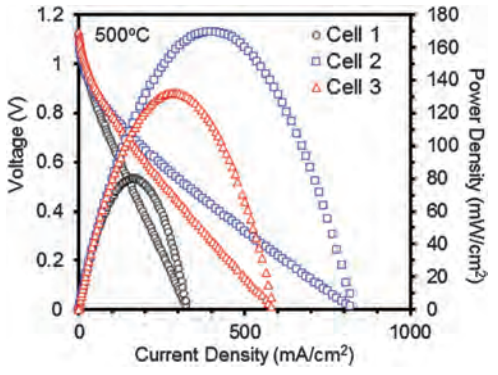

Fig. 4. *I–V* curves at 500 °C.

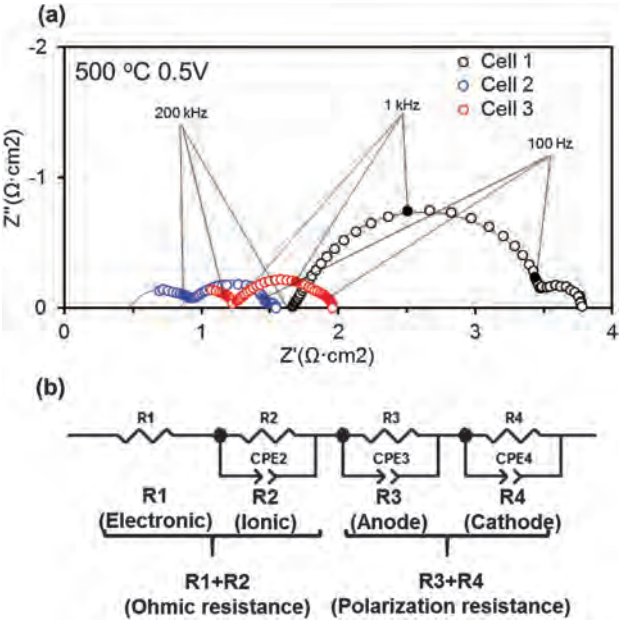

Fig. 5. (a) Nyquist plot of the impedance spectra under OCV at 500 °C and (b) EIS fitting model.

and cathode polarization resistance, respectively, in order of associated frequency ranges (higher to lower). The sum of high frequency resistances (R1 + R2) is independent of the bias voltage and thus can be interpreted as ohmic resistance, i.e., the sum of electronic (R1) and ionic (R2) resistances.[5] R1 + R2 were measured to be 1.69Ω · cm^2, 0.96Ω · cm^2, and 1.26Ω · cm^2 for cell 1, cell 2, and cell 3, respectively.

There was a clear distinction among ohmic resistances considering that the ionic resistances (R2) for the cells are identical. The clearly distinctive ohmic resistances seem to stem from the different electrical contact resistances (R1). The ohmic resistances significantly decreased when the Ni layer was added to the anode (cell 1 vs. cells 2/3). As previously mentioned, the Ag paste was connected to the bilayer anode and the current was collected from the anode. Schematic of the current collecting mechanism in the bilayer anode is shown in Figure 6. We speculate that there were two electron pathways from the TPBs region to the Ag paste. At cell 1, electrons are only transferred through pathway 1 (laterally through NiO-GDC). At cell 2 and cell 3, the Ni layer contributes to electron transport

Table II. Area–specific resistances of TF-SOFCs measured by EIS fitting model.

	Cell 1	Cell 2	Cell 3
R1+R2 (ohmic)	1.69 Ω · cm^2	0.96 Ω · cm^2	1.26 Ω · cm^2
R3 (Anode)	1.87 Ω · cm^2	0.38 Ω · cm^2	0.62 Ω · cm^2
R4 (Cathode)	0.19 Ω · cm^2	0.18 Ω · cm^2	0.18 Ω · cm^2

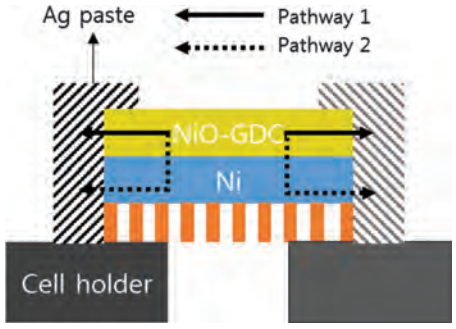

Fig. 6. Schematic of current collecting mechanism in the direct bilayer anode electron transfer to Ag paste (Pathway 1) via the Ni layer (Pathway 2).

at the anode by acting as a current collector so that the electronic resistance can be reduced.

Semicircles associated with the anode and cathode polarizations are also observed in the 200 kHz–100 Hz (intermediate frequency range) and <100 Hz (low frequency range) frequency ranges, respectively.[20, 27, 28] Considering all three cells have identical Pt cathodes, the difference in polarization resistance between cell 1 and cells 2–3 probably results from the anode side. Indeed, the cathode polarization resistances in all three cells at low frequency were identical at 0.18–0.19 $\Omega \cdot cm^2$. The anode polarization resistances of cell 1, cell 2, and cell 3 at intermediate frequency ranges were 1.87 $\Omega \cdot cm^2$, 0.38 $\Omega \cdot cm^2$, and 0.62 $\Omega \cdot cm^2$ under 0.5 V bias.

At the anode, the hydrogen oxidation reaction is known to occur in the following steps:[1]

(1) hydrogen gas molecule (H_2) adsorption onto the catalyst surface,

(2) dissociation of H_2 into hydrogen ions and electrons, and

(3) incorporation of hydrogen ions into the bulk electrolyte at TPB. Among these steps, step 2 (dissociation of H_2) is usually rate-determining.[1]

For cells 2–3, the hydrogen gas encounters the Ni layer before entering the porous NiO-GDC composites. In those cells, hydrogen molecules introduced into the anode may be more actively dissociated on the surface of the catalytic Ni surface than the case without the Ni layer. Hydrogen ions (protons) that are produced in such a manner may readily incorporate at the TPBs of the NiO-GDC composite. Although cells 2 and 3 may have lower TPB densities compared to cell 1 due to the thinner NiO, the anode polarization in those cells seem to largely benefit from fast hydrogen dissociation (Step 2), which results in smaller anode polarization resistances in cells 2 and 3 than in cell 1. In the meantime, a slight increase in anode polarization resistance in cell 3 compared to cell 2 (0.38 $\Omega \cdot cm^2 \rightarrow 0.62\ \Omega \cdot cm^2$) may imply high TPB density loss due to the thin NiO-GDC layer (70 nm) adversely affecting the anode polarization. Therefore, fuel cell performance decreases despite better catalytic activities.

4. CONCLUSION

NiO-GDC thin film anode performance for the TF-SOFCs was enhanced by inserting an additional Ni layer between the NiO-GDC and the substrate. The TF-SOFC with 210 nm-thick NiO-GDC layer and 70 nm-thick Ni layer exhibited the best performance with 170 mW/cm^2, which was more than a twofold increase compared to that with 280 nm-thick NiO-GDC only anode (80 mW/cm^2). The EIS analysis showed that such a performance increase was due to the reduced ohmic and anode polarization resistances, which benefitted from additional current collection and catalytic activity by the Ni layer, respectively. The fuel cell performance decreased when the NiO-GDC layer became too thin compared to the Ni layer due to TPB loss. These results provide the essential TF-SOFC design rules where a proper thickness combination of the NiO-GDC and Ni layers is essential for maximizing the TF-SOFCs performance when employing the bilayer anode.

Acknowledgments: This research was supported by the National Research Foundation of Korea (NRF) grant funded by the Korea government (MEST) (no. NRF-2011-0029576 and no. NRF-2013R1A1A2A10065234). The IAMD at Seoul National University and BK21 plus is also acknowledged for their partial support.

References and Notes

1. R. O'Hayre, S. W. Cha, W. Colella, and F. B. Prinz, Fuel Cell Fundamentals, 2nd edn., Wiley, New Yorks **(2009)**.
2. Y. Yoo, *J. Power Sources* 160, 202 **(2006)**.
3. S. Ji, I. Chang, G. Y. Cho, Y. H. Lee, J. H. Shim, and S. W. Cha, *Int. J. Hydrogen Energy* 39, 12402 **(2014)**.
4. J. Park, J. Y. Paek, I. Chang, S. Ji, S. W. Cha, and S. I. Oh, *CIRP Ann. - Manuf. Technol.* 62, 563 **(2013)**.
5. J. An, Y. B. Kim, J. Park, T. M. Gur, and F. B. Prinz, *Nano Lett.* 13, 4551 **(2013)**.
6. C. C. Chao, C. M. Hsu, Y. Cui, and F. B. Prinz, *ACS Nano* 5, 5692 **(2011)**.
7. K. Kerman, B. K. Lai, and S. Ramanathan, *J. Power Sources* 202, 120 **(2012)**.
8. D. Beckel, A. Bieberle-Hütter, A. Harvey, A. Infortuna, U. P. Muecke, M. Prestat, J. L. M. Rupp, and L. J. Gauckler, *J. Power Sources* 173, 325 **(2007)**.
9. L. R. Pederson, P. Singh, and X. D. Zhou, *Vacuum* 80, 1066 **(2006)**.
10. W. Z. Zhu and S. C. Deevi, *Mater. Sci. Eng. A* 362, 228 **(2003)**.
11. H. J. Hwang, J. W. Moon, S. Lee, and E. A. Lee, *J. Power Sources* 145, 243 **(2005)**.
12. K. R. Reddy and K. Karan, *J. Electroceramics* 15, 45 **(2005)**.
13. V. A. C. Haanappel, A. Mai, and J. Mertens, *Solid State Ionics* 177, 2033 **(2006)**.
14. J. B. Goodenough and Y. H. Huang, *J. Power Sources* 173, 1 **(2007)**.
15. T. Ishihara, T. Shibayama, H. Nishiguchi, and Y. Takita, *Solid State Ionics* 132, 209 **(2000)**.
16. J. Ayawanna, D. Wattanasiriwech, S. Wattanasiriwech, and K. Sato, *Mater. Manuf. Processes* 29, 767 **(2014)**.
17. M. Kim, Y. C. Ha, T. N. Nguyen, H. Y. Choi, and D. Kim, *Nanotechnol.* 24, 505304 **(2013)**.
18. S. Ji, I. Chang, I, Y. H. Lee, M. H. Lee, and S. W. Cha, *Thin Solid Films* 539, 117 **(2013)**.

ARTICLE

19. S. Ji, I. Chang, Y. H. Lee, J. Park, J. Y. Paek, M. H. Lee, and S. W. Cha, *Nanoscale Res. Lett.* 8, 48 **(2013)**.
20. J. Park, I. Chang, J. Y. Paek, S. Ji, W. Lee, S. W. Cha, and J. M. Lee, *CIRP Ann. - Manuf. Technol.* 63, 513 **(2014)**.
21. J. Park, Y. Lee, I. Chang, W. Lee, and S. W. Cha, *Thin Solid Films* 584, 125 **(2014)**.
22. M. Mukhopadhyay, J. Mukhopadhyay, A. D. Sharma, and R. N. Basu, *Int. J. Hydrogen Energy* 37, 2524 **(2012)**.
23. C. Xia and M. Liu, *Solid State Ionics* 152–153, 423 **(2002)**.
24. C. W. Kwon, J. W. Son, J. H. Lee, H. M. Kim, H. W. Lee, and K. B. Kim, *Adv. Funct. Mater*. 21, 1154 **(2011)**.
25. S. Ha, P. C. Su, and S. W. Cha, *J. Mater. Chem. A* 1, 9645 **(2013)**.
26. I. Chang, S. Woo, M. H. Lee, J. H. Shim, Y. Piao, and S. W. Cha, *Appl. Surf. Sci.* 282, 463 **(2013)**.
27. S. B. Adler, *Solid State Ionics* 111, 125 **(1998)**.
28. T. Yamaguchi, H. Sumi, K. Hamamoto, T. Suzuki, Y. Fujishiro, J. D. Carter, and S. A. Barnett, *Int. J. Hydrogen Energy* 39, 19731 **(2014)**.

ARTICLE